Physics Letters B 748 (2015) 117–124

Contents lists available at ScienceDirect

Physics Letters B

www.elsevier.com/locate/physletb

Classical dynamics of the Abelian Higgs model from the critical point and beyond

G.C. Katsimiga, F.K. Diakonos, X.N. Maintas

Department of Physics, University of Athens, GR-15784 Athens, Greece

ARTICLE INFO

Article history:
Received 3 April 2015
Accepted 26 June 2015
Available online 2 July 2015
Editor: A. Ringwald

ABSTRACT

We present two different families of solutions of the U(1)-Higgs model in a $(1+1)$ dimensional setting leading to a localization of the gauge field. First we consider a uniform background (the usual vacuum), which corresponds to the fully higgsed-superconducting phase. Then we study the case of a non-uniform background in the form of a domain wall which could be relevantly close to the critical point of the associated spontaneous symmetry breaking. For both cases we obtain approximate analytical nodeless and nodal solutions for the gauge field resulting as bound states of an effective Pöschl–Teller potential created by the scalar field. The two scenaria differ only in the scale of the characteristic localization length. Numerical simulations confirm the validity of the obtained analytical solutions. Additionally we demonstrate how a kink may be used as a mediator driving the dynamics from the critical point and beyond.

1. Introduction

Solitons come in two "flavors" namely non-topological and topological ones. Their physical meaning as well as their mathematical properties have been vastly studied in the literature, both in the context of field theories and cosmology but also in condensed matter physics. Non-topological solitons are found as localized "lumps" [1], Q-balls [2] or oscillons [3] while topological solitons may have the form of instantons [4], monopoles [5–7], vortices [8,9] or domain walls [10]. Composite objects, such as (non-) Abelian gauge fields localized on domain walls [11] and monopoles confined by vortices [12] among others, arise in gauge theories with spontaneous symmetry breaking. In many cases an explicit analytical soliton solution of the respective theory is not possible, and the properties of solitons are obtained by performing numerical simulations [13]. The latter are usually accompanied by some analytical approximation [14] e.g. by considering the asymptotic behavior of the fields.

The simplest topological defect with an analytical expression is a domain wall (alias kink) in $(1+1)$ dimensions for a single scalar field, which is studied thoroughly in the sine-Gordon and the ϕ^4 model, and still attracts interest, see e.g. the very recent works of kink-kink interactions of Refs. [15,16] or of Ref. [17] for kinks in a ϕ^6 model. Domain walls and their interactions are also considered in supersymmetric theories where more than one scalars are involved, and families of such walls link various supersymmetric vacua [18,19]. Kink solutions may also be used for modeling fluxons [20] or describing phase-slips in superconductors, where the phase of the order parameter periodically drops by 2π in a single point (see e.g. [21] or the more recent results of [22–24]).

An important feature regarding topological defects is that they may be used as a mechanism inducing localization. Such examples include the localization of fermions on a kink [25,26], which constitutes a trapping mechanism for fermionic zero modes, and also the formation of localized gauge bosons on a domain wall [11] with implications in the process of dynamic compactification. More recently the localization of a spin-0 field [27] was induced by a kink-lump solution of two scalars leading to resonant behavior relevant to gravity in warped space–times [28].

Although localized structures on a non-vanishing vacuum share common properties with oscillons trapped by topological defects, there is no link between these two different solutions up to now. In the present work we will attempt to establish such a connection in the framework of $(1+1)$ dimensional Abelian–Higgs [29,30] model. Such a theory, although simple, can describe both non-topological (oscillon [31]) and topological (domain wall [10]) solutions. As we will show below, both solutions (oscillons, kinks) generate an effective Pöschl–Teller [32,33] potential leading to the localization of the respective gauge field. Additionally we provide

E-mail address: liakatsim@gmail.com (G.C. Katsimiga).

http://dx.doi.org/10.1016/j.physletb.2015.06.065

a whole "family" of gauge field configurations exhibiting nodes in their profiles emerging as bound states of the aforementioned potential. These nodal solutions are long lived and robust and may be interpreted as oscillon excitations. Furthermore we show how a "moving" kink may dynamically localize a gauge field in the bulk depending on its initial energy. We argue that this process can be interpreted in terms of the dynamics near the critical point and we demonstrate how the traveling kink can drive the pathway from a globally symmetric vacuum state to the phase of a non-vanishing vacuum with globally spontaneously broken symmetry.

The paper is organized as follows: in Section 2 we write the equations of motion and their exact vacuum solutions, corresponding to the uniform [the scalar field profile attains a globally constant vacuum expectation value (vev)] and the non-uniform backgrounds (the scalar field is a domain wall). In Section 3 we show how the oscillons on top of the vev lead to localized solutions for the respective gauge field, using an approximate perturbation method. A standard perturbation scheme is employed in Section 4, and analytical solutions of a small amplitude gauge field, around the domain wall of the non-uniform background, are presented. These families of solutions are shown to have different characteristic length scale than that of the solutions in the uniform background. In both sections numerical simulations verify our analytical results and imply the robustness of the solutions. A more detailed comparison/connection between the two different regimes and the respective solutions is presented in Section 5 where we also show numerical results demonstrating that a localized solution around the domain wall may be obtained by a moving soliton in the bulk. Our conclusions are presented in Section 6.

2. Lagrangian and equations of motion

We consider classical electrodynamics in flat Minkowski space–time described by the gauge invariant Lagrangian $\mathcal{L}$:

$$\mathcal{L} = -\frac{1}{4}F_{\mu\nu}F^{\mu\nu} + (D_\mu\Phi)^*(D^\mu\Phi) - V(\Phi^*\Phi), \tag{1}$$

where Φ is a charged scalar field interacting with the gauge field A_μ and $V(|\Phi|)$ is the double well potential $V(|\Phi|) = \lambda|\Phi|^4 + \mu^2|\Phi|^2$. The covariant derivative is defined as $D_\mu = \partial_\mu + ieA_\mu$, e is the coupling constant and $F_{\mu\nu}$ is the electromagnetic tensor. The Hamiltonian (energy density) of the above system is given by:

$$\begin{aligned}\mathcal{H} &= \frac{\partial\mathcal{L}}{\partial(\partial_0\Phi)}\partial_0\Phi + \frac{\partial\mathcal{L}}{\partial(\partial_0\Phi^*)}\partial_0\Phi^* + \frac{\partial\mathcal{L}}{\partial(\partial_0 A_\nu)}\partial_0 A_\nu - \mathcal{L} \\ &= \frac{1}{2}\left[|B|^2 + |E|^2\right] + |\pi|^2 + |\mathbf{D}\Phi|^2 + V,\end{aligned} \tag{2}$$

where in the last expression we have explicitly used the physical fields $\mathbf{E} = -\partial_t A - \nabla A_0$ (electric), $\mathbf{B} = \nabla \times A$ (magnetic) and $\pi \equiv D_0\Phi$. Although our analysis will be given with respect to Φ and A, the connection with the electromagnetic field is necessary for the interpretation of our results.

For a $(1+1)$ dimensional setting, we consider the following ansatz for the gauge field A_μ: $A_0 = A_1 = A_3 = 0$, $A_2 = A(x,t)$, i.e. a linearly polarized (in the z axis) magnetic field propagating in the x direction. For $\mu^2 < 0$ the symmetry is spontaneously broken and the scalar field acquires a non-vanishing vacuum expectation value (vev). Choosing the unitary gauge in which the Φ field is real, its vev is $\Phi = \pm\upsilon$, where $\upsilon^2 = -\mu^2/\lambda$. Given the previous assumptions, the electromagnetic tensor has non-vanishing components $F_{0\nu} \equiv F_{02} = \partial_t A_2$, $F_{i\nu} \equiv F_{12} = \partial_x A_2$ and the equations of motion stemming from the above Lagrangian are:

$$\Box\Phi - \mu^2\Phi + \lambda\Phi^3 + e^2\Phi A^2 = 0, \tag{3}$$

$$\Box A + e^2\Phi^2 A = 0. \tag{4}$$

The potential in terms of the fields Φ and A is $V(\Phi, A) = (\lambda/4)\left(\Phi^2 - \upsilon^2\right)^2 + (e^2/2)\Phi^2A^2$, where we have added a constant $\sqrt{\lambda}\upsilon^2/2$ in order to complete the square in the first term. The symmetric phase, with respect to reflection symmetry, corresponds to a single minimum:

$$\Phi = 0, \qquad A = 0, \tag{5}$$

and breather solutions are not supported by the system, while in the broken phase the system of Eqs. (3)–(4) admits the following exact solutions:

$$\Phi = \pm\upsilon, \quad A = 0, \tag{6}$$

$$\Phi = \pm\upsilon\tanh\left(\sqrt{2\lambda}\upsilon x/2\right) \equiv \phi_k, \quad A = 0, \tag{7}$$

where Eq. (6) is the zero energy solution $E_{min} = 0$ corresponding to a homogeneous scalar field (uniform vacuum). On the other hand Eq. (7) is an inhomogeneous solution (non-uniform background) with a finite energy per unit area $E_{kink} = 2\sqrt{2\lambda}\upsilon^3/3$. The latter is the well known kink solution of the ϕ^4 model, which has been studied in a variety of physical contexts (see e.g. Refs. [4,10] for a field theory approach, Ref. [34] for kinks in condensed matter physics and Ref. [9] for kinks and other topological defects in cosmology). Since the energy difference of the above solutions is analogous to υ^3, their energies are comparable for $\upsilon \to 0^+$ near the critical point i.e. just after symmetry breaking.

Below we will search for localized low energy solutions for both the scalar and the gauge field in the following two cases: (i) in the uniform vacuum case and (ii) in the non-uniform background around the kink's core.

In what follows, we express Eqs. (3)–(4) in a dimensionless form by rescaling space–time coordinates and fields as $x \to e\upsilon x$, $t \to e\upsilon t$, $\Phi \to \upsilon\phi$ and $A \to \upsilon A$. However for the interpretation of our findings we will always refer to the physical units. After rescaling we obtain the following set of equations:

$$\Box\phi + \frac{q^2}{2}\phi^3 - \frac{q^2}{2}\phi + \phi A^2 = 0, \tag{8}$$

$$\Box A + \phi^2 A = 0, \tag{9}$$

where $q \equiv \sqrt{2\lambda/e^2}$ is the single parameter of the system and the energy density becomes:

$$\mathrm{E} = \frac{1}{2}(\partial_t\phi)^2 + \frac{1}{2}(\partial_x\phi)^2 + \frac{1}{2}(\partial_t A)^2 + \frac{1}{2}(\partial_x A)^2 + \mathrm{V}, \tag{10}$$

with

$$\mathrm{V} = \frac{q^2}{8}(\phi^2 - 1)^2 + \frac{1}{2}\phi^2A^2. \tag{11}$$

3. Solutions around the uniform vacuum

3.1. Analytical considerations – multiscale expansion

In this section we search for small amplitude localized solutions in the bulk of the classical vacuum Eq. (6) and far beyond the critical point, i.e. when $\upsilon \gg 1$ and in dimensionless form $\phi = \pm 1$. Although we show results only for $\phi = 1$ analogous results hold for $\phi = -1$ due to the reflection symmetry of the potential. This scenario corresponds to the fully higgsed – "superconducting" phase – [11].

In order to find a localized solution of the non-integrable system of Eqs. (8)–(9), we will use a multiscale perturbation expansion [35]. While the details of this method are given in Appendix A, here we briefly comment on its basic ingredients. The

multiscale expansion introduces different space–time scales (fast and slow) and a carrier wave solution in the fast scale is obtained in the linear limit. Then the envelope of this wave, which is considered to evolve in the slow scales, is found to travel with the group velocity of the plane wave and satisfies a solvable nonlinear equation at some higher order.

In our case we will use the following asymptotic expansion

$$\phi = 1 + \epsilon\phi^{(1)} + \ldots, \quad A = 0 + \epsilon^2 A^{(2)} + \ldots, \tag{12}$$

where $\phi^{(i)}$ $(i = 1, 2, 3, \ldots)$ describe the perturbations of the scalar field on top of the vev, $A^{(i)}$ is the small amplitude gauge field and $\epsilon \ll 1$ is a formal small parameter. In the first order of the expansion $\mathcal{O}(\epsilon)$ for ϕ and in the second order for A, $\mathcal{O}(\epsilon^2)$, the solutions correspond to the following plane waves:

$$\phi^{(1)} = u(x_1, t_1, x_2, t_2, \ldots)e^{i(k_1 x - \omega_1 t)} + \text{c.c}, \tag{13}$$

$$A^{(2)} = \mathrm{v}(x_1, t_1, x_2, t_2, \ldots)e^{i(k_2 x - \omega_2 t)} + \text{c.c}, \tag{14}$$

where "c.c" stands for the complex conjugate. The wavenumbers $k_{1,2}$ and frequencies $\omega_{1,2}$ are connected through the dispersion relations $\omega_1 = \sqrt{k_1^2 + q^2}$, $\omega_2 = \sqrt{k_2^2 + 1}$. The envelope functions u and v are yet arbitrary in this order. In the next order of the expansion ($\mathcal{O}(\epsilon^2)$ for ϕ and $\mathcal{O}(\epsilon^3)$ for A), the compatibility conditions dictate that the envelopes move with the respective group velocities $v_g^{(1,2)} = d\omega_{1,2}/dk_{1,2}$. In what follows and without loss of generality we restrict our analysis in the case of zero group velocity ($k_1 = k_2 = 0$) and thus the envelopes are functions of (x_1, t_2). However we note that for finite group velocities we obtain results that are quantitatively the same describing traveling solutions.

At the orders $\mathcal{O}(\epsilon^3)$ for the envelope $u(x_1, t_2)$, and $\mathcal{O}(\epsilon^4)$ for the envelope $\mathrm{v}(x_1, t_2)$ we find:

$$iq\partial_{t_2} u = -\frac{1}{2}\partial_{x_1}^2 u - 3q^2|u|^2 u, \tag{15}$$

$$i\partial_{t_2}\mathrm{v} = -\frac{1}{2}\partial_{x_1}^2 \mathrm{v} + V(x_1)\mathrm{v}, \quad V(x_1) = -\alpha|u|^2, \tag{16}$$

where in Eq. (16) $\alpha(q) = 2(6 - q^2)/(4 - q^2)$ while Eq. (15) is the well known focusing (i.e. with positive relative sign between the dispersion and the nonlinearity) NLS equation. The latter admits bright soliton solutions [36] in the form:

$$u = u_0 \mathrm{sech}\,(\mathrm{w}x_1)\, e^{i\frac{\mathrm{w}^2}{2q}t_2}, \tag{17}$$

where u_0 is a free parameter characterizing the amplitude of the soliton, $\mathrm{w} = \sqrt{3}qu_0$ is its inverse width. This way we have constructed a localized solution for the $\phi^{(1)}$ field [cf. Eq. (13)].

For the above solutions of $u(x_1, t_2)$, Eq. (16) becomes a linear Schrödinger equation for the envelope $\mathrm{v}(x_1, t_2)$, in the presence of the effective Pöschl–Teller potential $V(x_1) \sim \mathrm{sech}^2(x_1)$. The strength α and in particular its sign, depend only on the parameter q. In particular for $q \in (0, 2)$ and $q > \sqrt{6}$ the parameter α is positive and $V(x_1)$ has the form of a sech-shaped well. As such, in this parameter regime one can obtain localized solutions for $\mathrm{v}(x_1, t_2)$ corresponding to a localized gauge field A. Bounded solutions of Eq. (16) can be found using the ansatz: $\mathrm{v}(x_1, t_2) = \hat{\mathrm{v}}(x_1)\exp[-i(E/2)t_2]$ where $E/2$ is the energy eigenvalue. Substituting the above in Eq. (16) we obtain a Sturm–Liouville equation of the following form:

$$\partial_{x_1}^2 \hat{\mathrm{v}}(x_1) + \left(E + 2\alpha\,\mathrm{sech}^2(\mathrm{w}x_1)\right)\hat{\mathrm{v}}(x_1) = 0. \tag{18}$$

Equation (18) can be transformed into the *associated Legendre* equation by making the substitution $T = \tanh(\mathrm{w}x_1)$ which can then be solved analytically. In fact, for each value of the parameter q there exist a total number of N bound solutions with E_n $(n = 0, 1 \ldots, N - 1)$ discrete energy eigenvalues, both given in terms of the functions:

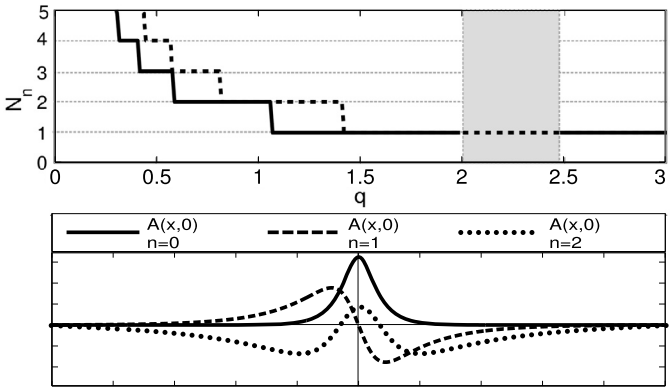

Fig. 1. (Color online.) Top panel: Total number of bound states $N(q)$ for the uniform vacuum are shown with the solid line and for the non-uniform background with the dashed line. Gray box indicates the region $2 < q < \sqrt{6}$ where no bound states exist in the uniform case. Bottom panel: Profiles of a nodeless ($n = 0$) state depicted with solid black line and the nodal ones, where the first excited state ($n = 1$) is plotted with a dashed black line and the second excited ($n = 2$) with the dotted black line. For all cases $q = 1/2$.

$$f_N(z) = \left[(z + 1/4)^{1/2} - 1/2\right] + 1, \tag{19}$$

$$f_E(z) = -\frac{1}{z}\left((z + 1/4)^{1/2} - (n - 1/2)\right)^2, \tag{20}$$

where in Eq. (19), "[ ]" denotes the integer part. From the aforementioned substitutions it follows that in the case of the uniform background both N and E_n are given by the expressions:

$$N = f_N\left(\frac{2\alpha}{\mathrm{w}^2}\right), \quad E_n = -2\alpha\, f_E\left(\frac{2\alpha}{\mathrm{w}^2}\right). \tag{21}$$

Furthermore the localized solutions of the envelope $\mathrm{v}(x_1, t_2)$ are given by the so-called *associated Legendre functions* [37] as follows:

$$\hat{\mathrm{v}}_n(x_1) = P_\rho^\sigma\left(\tanh(\mathrm{w}x_1)\right), \tag{22}$$

where σ and ρ are related to the energy and potential coefficients through the relations: $\sigma^2 = -E_n$, and $\rho^2 + \rho = 2\alpha/\mathrm{w}^2$. In the top panel of Fig. 1, we show the total number of bound states N as a function of q. In the region $q < 2$, as q decreases the number of bound states increases, for $q > \sqrt{6}$ only one such state exists, while for $2 < q < \sqrt{6}$ only scattering states are found (indicated by the gray box) [30].

We can now write the approximate solutions for fields ϕ and A as:

$$\phi(x, t) \approx 1 + \epsilon u_0 \mathrm{sech}\,(\mathrm{w}\epsilon x)\left(e^{-i(\omega_1 - \epsilon^2\mathrm{w}^2/2q)t} + \text{c.c}\right), \tag{23}$$

$$A(x, t) \approx \epsilon^2 \hat{\mathrm{v}}_n(\epsilon x)\left(e^{-i(\omega_2 + \epsilon^2 E_n/2)t} + \text{c.c}\right), \tag{24}$$

and $\hat{\mathrm{v}}_n$ is given by Eq. (22). We have thus shown that, in this regime of a small gauge field A, the localized perturbations of ϕ (due to self interactions) upon the vev, act as an effective potential within which the gauge field can be localized. More importantly we note the following: our result of Eq. (24) in the case of $n = 0$ corresponds to an "oscillon" solution for the gauge field with the usual sech-shaped (nodeless) envelope. Such oscillons have been shown to exist in various settings [38,39] and their properties (stability and robustness) have been extensively studied. However

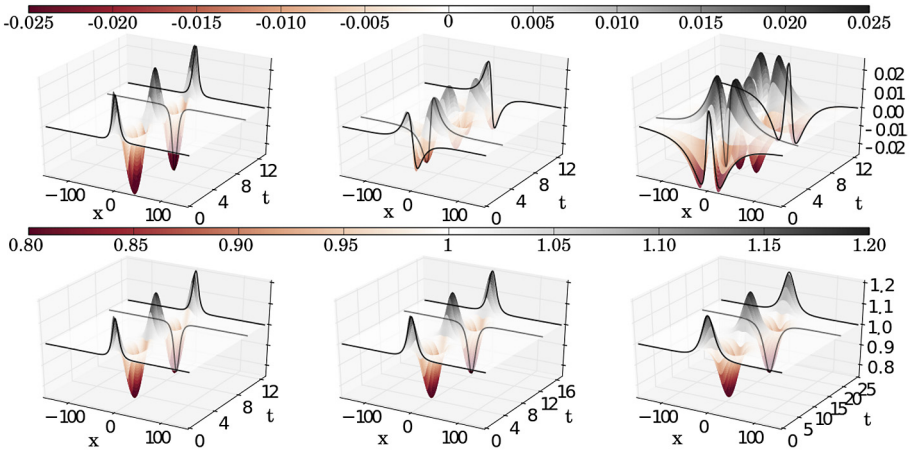

Fig. 2. (Color online.) Top row: 3d plots showing $t = 2T$ oscillation periods for $A(x,t)$ for $n = 0$, $q = 1$ (left), $n = 1$, $q = 3/4$ (middle) and $n = 2$, $q = 1/2$ (right). Bottom row: 3d plots depicting the field $\phi(x,t)$ for each of the above A's. For the uniform vacuum.

for larger values of $n = 1, 2, 3, \ldots$ the solutions in Eq. (24) correspond to localized oscillating structures with a finite number of nodes-*nodal oscillons*-which as far as we know have not been yet recognized as such in the literature. The analytical result of Eq. (24) for $t = 0$ is plotted in the bottom panel of Fig. 1 for the nodeless case $n = 0$, and for the first and second excited states ($n = 1$ and $n = 2$ respectively). Below we will employ direct numerical simulations in order to study the robustness and longevity of these structures. It is worthwhile at this point to stress out that the oscillon solutions presented above, owe their existence to the spontaneous breaking of the global reflection symmetry leading to $\langle\phi\rangle \neq 0$, in contrast to the symmetric phase of Eq. (5) for which $\langle\phi\rangle = 0$ and no breather solutions exist. Furthermore, since the scalar field attained its non-vanishing vev, this scenario corresponds to the fully-higgsed superconducting phase far beyond the associated critical point. The localized excitations of the scalar field induce localization to the respective gauge field leading in turn to a vanishing magnetic field in this region.

3.2. Numerical results: uniform vacuum

In this section numerical results are presented, concerning the evolution of the approximate solutions obtained in Eqs. (23)–(24). In particular we perform direct integration of Eqs. (8)–(9) using as initial conditions Eqs. (23)–(24) at $t = 0$. In all numerical results presented below we use lattice spacing $dx = 0.2$, time step $dt = 0.01$ and the total time of integration is of order $t \sim 10^4$ which corresponds to $\sim 10^4$ oscillations for the fields.

In Fig. 2 we show the evolution during two full periods in time $t = 2T_i$, where $T_{1,2} = 2\pi/\omega_{1,2}$ for the scalar and the gauge field respectively. The left column corresponds to the case of the nodeless oscillon ($n = 0$) for $q = 1$. Both fields have similar structure but different frequencies; also note that in order for the multiscale expansion to be valid, the width of both fields is restricted to be of the order $\mathcal{O}(10^1)$. The middle column of this figure shows a new mode for the gauge field A with one node ($n = 1$) for $q = 3/4$, while the right column shows the second excited state ($n = 2$) of Eq. (18) in both cases the scalar field is still sech-shaped.

We have confirmed the robust evolution of such states for times up to $t \sim 10^4$. In Fig. 3 contour plots of the energy density Eq. (10) for different values of q and for both the nodeless and nodal oscillons are given. Although the more usual case of a nodeless soliton is somehow expected to be robust in the one-dimensional setting, the robustness of the higher excited states is not necessarily expected.

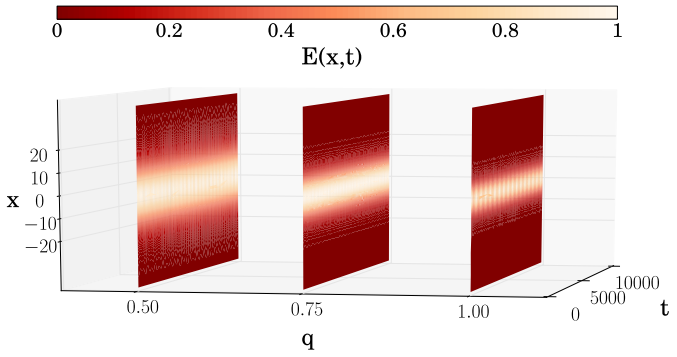

Fig. 3. (Color online.) 3d plots showing the normalized, with respect to its maximum value, energy density $E(x,t)$ for different values of the parameter q and for total time of integration in each case of $t = 10^4$ in the uniform vacuum.

4. Solutions around the non-uniform background

4.1. Analytical considerations-perturbation around kink's core

Main subject of this section is to obtain localized solutions to the system of Eqs. (8)–(9) around the core of the domain wall. Since the width of the domain wall is of order $\mathcal{O}(1)$, and we are interested in finding localized solutions for the gauge field due to the presence of the domain wall, instead of using a slow-scale approximation we consider the following perturbation expansion:

$$A = 0 + \epsilon A^{(1)}, \quad \phi = \phi_k + \epsilon^2 \tilde{\phi}. \tag{25}$$

In the above expression $A^{(1)}$ is the unknown, small amplitude gauge field, ϕ_k is the exact kink solution of Eq. (7), and $\tilde{\phi}$ describes higher order perturbations upon the kink due to the presence of $A^{(1)}$ [cf. Eqs. (8)–(9)]. Note that in Eq. (25), corrections to the scalar field of order ϵ are not included, since such terms describe perturbations around the kink, decoupled from the gauge field, which were studied in Ref. [40]. On the other hand our analysis, as well as our expansion, concerns the effects of a small amplitude gauge field $A^{(1)}$.

Substituting the expansion of Eq. (25) into the system of Eqs. (8)–(9), at leading order (i.e. to the order ϵ) we obtain the following equation for the small amplitude gauge field:

$$\Box A^{(1)} + \phi_k^2 A^{(1)} = 0. \tag{26}$$

Notice that the stationary kink solution ϕ_k acts as an effective potential for the field $A^{(1)}$. Furthermore, we look for solutions of

the form: $A^{(1)}(x,t) = \exp[-i\omega t]\hat{A}^{(1)}(x)$, where ω is the frequency while $\hat{A}^{(1)}(x)$ is a function depending on the spatial coordinate x. Substituting the aforementioned ansatz into Eq. (26) we obtain the eigenvalue problem:

$$\partial_x^2 \hat{A}^{(1)} + \left(E + \mathrm{sech}^2(qx/2)\right)\hat{A}^{(1)} = 0, \tag{27}$$

where $E = \omega^2 - 1$ is the corresponding eigenvalue. It is readily seen that Eq. (27) is identical to equation (18) and thus *localized* solutions of $\hat{A}^{(1)}$ can be found as the bound states of the above equation given by:

$$\hat{A}_n^{(1)}(x) = P_\rho^\sigma\left(\tanh(qx/2)\right). \tag{28}$$

The total number of bound states (cf. dashed black line in Fig. 1) and the energy spectrum are now given by

$$N = f_N\left(\frac{4}{q^2}\right), \quad E_n = f_E\left(\frac{4}{q^2}\right), \tag{29}$$

while the corresponding approximate solutions for A can be written as:

$$A(x,t) \approx \epsilon \hat{A}_n^{(1)}(x)\left(e^{-iE_n t} + \mathrm{c.c}\right). \tag{30}$$

The above solutions correspond to a family of localized gauge fields centered at the domain wall having the form of nodeless and nodal oscillon-like structures supported by an effective potential due to the presence of the kink. These oscillons are of small amplitude and have a spatial width of the order of the corresponding domain wall (which dependents on q). Although these solutions bare many similarities with the solutions obtained in Section 3, they are characterized by in a different length scale, and their localization mechanism is fundamentally different. In particular the effective potential in Eq. (27), is due to the presence of the time-independent, exact solution of the original system of equations, while the effective potential in Eq. (18) is due to an approximate oscillon. In particular the case of the non-uniform background discussed in this section corresponds to a scenario just after the symmetry breaking, and thus close to the critical point $\phi = 0$. The kink interpolates between the just formed wells of the potential connecting them, and since q is relatively small, the solutions obtained above are not energetically disfavored. Furthermore, since the vacua are degenerate and close to the vacuum of the unbroken phase, the order parameter, having the form of the kink, induces localization of the respective gauge field leading to a vanishing magnetic field around kink's core. Below we will attempt to establish a connection between these two scenaria.

4.2. Numerical results: non-uniform background

In the preceding section we obtained families of nodeless and nodal oscillon-like structures. In what follows, we will elaborate on how the aforementioned solutions evolve in time, so as to verify the validity as well as the robustness of our analytical findings. In particular we will perform numerical integration of the system of equations (8)–(9) using as initial conditions, (at $t = 0$), the exact domain wall solution of Eq. (7) and Eq. (30).

In the left column of Fig. 4 a 3d plot shows the first two oscillations for a sech-shaped gauge field (top), i.e. a nodeless ($n = 0$) oscillon, for $q = 1$ and its profile at $t = 0$ is indicated with a solid black line. The scalar field corresponding to the above oscillon is also depicted in the bottom panel of the same column. Since $\phi(x,t)$ is non-oscillating, the main contribution for such a state comes from the leading order kink solution ϕ_k. Accordingly, in the middle and right columns of Fig. 4 top panels depict the field $A(x,t)$ corresponding to the first excited state, ($n = 1$ solution), for $q = 3/4$ and second excited state ($n = 2$) for $q = 1/2$ respectively. The corresponding scalar fields are also plotted in the bottom panel of each column. In both cases the kink solution is slightly affected by the small amplitude perturbations considered here. Both nodeless and nodal oscillons remain robust for at least $t \sim 10^4$ total time of integration and for different values of the parameter q. In order to highlight the longevity as well as the robustness of the oscillons obtained in this limit, in Fig. 5 a 3d plot consisting from three energy density contours is depicted for $t = 10^4$.

We have thus verified that in the non-uniform case a small amplitude gauge field alters the exact kink solution at order ϵ^2, as per our analytical findings of Eq. (30). As such, the kink supports not only the standard nodeless oscillons but also the nodal ones, which in turn remain localized throughout all our simulations. Additionally, these novel structures seem to expel smaller amounts of radiation when compared to the nodal oscillons of the uniform vacuum case.

5. Dynamical localization of the gauge field

Our previous analysis was guided by two configurations of the scalar field: the uniform non-zero vacuum and the kink state. As already mentioned, these two states describe different physical scenaria and seem to be dynamically disconnected. However, just after a spontaneous symmetry breaking, when υ is very small, the uniform non-zero vacuum is energetically almost degenerate with the kink configuration and the dynamics may support mixed configurations combining characteristics of both scenaria.

In order to develop a physical picture for this particular case, let us focus on the scalar field and its ground state. When the reflection symmetry $\phi \to -\phi$ is restored the ground state is the uniform configuration $\phi = 0$. To make a clearer connection with the phase transition induced by the spontaneous symmetry breaking of the reflection symmetry in this self-interacting scalar field theory, let us define as an order parameter of the transition the space averaged value of the scalar field: $\langle\phi\rangle_V = \frac{1}{V}\int_V dx\phi(x)$, where $\phi(x)$ is a static field configuration minimizing the energy functional of the field ϕ. For the symmetric phase ($\langle\phi\rangle = 0$) any localized excitation of this configuration in the form of an oscillon is unstable and dies out as time evolves.

Consider now the case when the reflection symmetry is spontaneously just broken. Then the ground state of the field becomes doubly degenerate ($\pm\upsilon$) with υ close to zero. The uniform states $\phi(x) = \upsilon$ or $\phi(x) = -\upsilon$ are energetically almost degenerate with the kink configuration $\phi(x) = \upsilon\tanh\left(\sqrt{2\lambda}\upsilon x/2\right)$. Due to this approximate degeneracy we extend the definition of the order parameter allowing in the averaging also the use of the kink configuration. Of course also the order parameter values for all these configurations are almost degenerate. However, an important issue concerning symmetry breaking is that the kink configuration is characterized by vanishing order parameter $\langle\phi\rangle = 0$ while the two degenerate vacua have $\langle\phi\rangle \neq 0$. Thus the kink is a topological structure allowing the communication between the two vacua, breaking the symmetry locally but not globally i.e. at the level of the order parameter. In this sense one can interpret the kink as a fluctuation of the reflection symmetric vacuum $\phi(x) = 0$ leading to a local symmetry breaking before a global breaking of the reflection symmetry establishes.

When the energy difference between the uniform vacuum states ($\pm\upsilon$) and the kink is very small, then the latter may be entropically favored constituting the representative of the field fluctuations driving the transition from the globally unbroken to

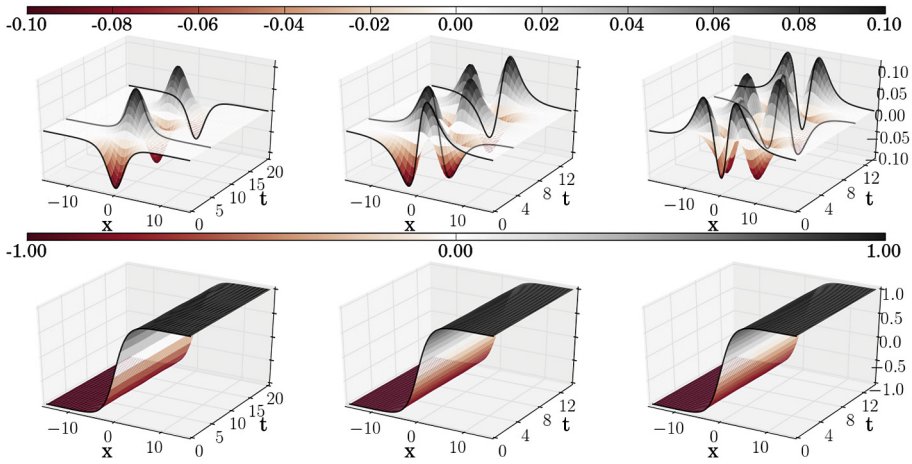

Fig. 4. (Color online.) Top row: 3d plots showing $t = 2T$ oscillation periods for $A(x,t)$ for $n = 0$, $q = 1$ (left), $n = 1$, $q = 3/4$ (middle) and $n = 2$, $q = 1/2$ (right). Bottom row: 3d plots depicting the field $\phi(x,t)$ for each of the above A's. For the non-uniform background.

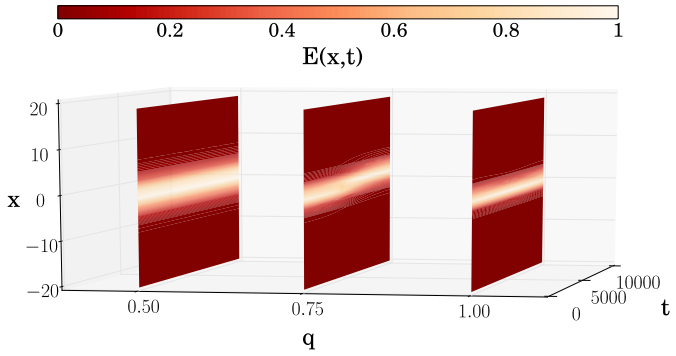

Fig. 5. (Color online.) Same as Fig. 3 but for the non-uniform background.

the globally broken phase of the reflection symmetry. Adopting this point of view, one can now naturally ask how localized, time dependent fluctuations (breathers) of the kink, which may cause the dynamical establishment of the non-vanishing order parameter value, evolve in time.

This is the issue we will consider in this section taking into account also the presence of the gauge field. Furthermore we will consider also the case when the kink is traveling with a velocity v_k. This is a dynamical process connecting snapshots consisting of different static kink configurations with equal energy. These different configurations could be interpreted as the origin of the entropic dominance of the kink soliton close to the critical point. Stability of localized fluctuations is such a time dependent background would signal the validity of the attempted critical dynamics description. Note that the soliton solutions of the preceding sections may have the form of traveling waves by applying a Lorentz boost. In our numerical simulations a moving kink is realized as follows: $\phi_k = \tanh[\gamma q(x - v_k t)/2]$, where v_k is the velocity of the kink and $\gamma = 1/\sqrt{1 - v_k^2}$ is the Lorentz factor [10]. The relevant nodeless solitons in the bulk are given by Eqs. (23)–(24) and are not traveling.

We have performed various realizations of the above configurations in a numerical experiment for different values of q and for different velocities. The results are summarized as follows. A direct relation between the possible outcome of the collision and the velocity of the domain wall (thus its kinetic energy) is observed. In fact we found that for any q, there is a lower critical velocity, above which the gauge field is localized on the domain wall. Additionally, depending on the value of q and the possible nodal (excited) states [cf. top panel of Fig. 1], as the velocity of the kink increases the higher excited state is realized. The above result can, at least qualitatively, be explained from energetic considerations. For small velocities, the kinetic energy of the kink is not sufficient in order to generate the lower possible bound state of the eigenvalue problem (27), and thus a lower critical velocity exists. Also the larger the velocity of the moving domain wall, the more energy is transferred to the gauge field and the higher excited states can then be formed. Importantly after the collision the original localized oscillon in the bulk remains intact, and undergoes a phase-shift [41]. This shift is found to be velocity dependent in a similar manner to the outcome of soliton collisions (see Refs. [15,42]).

The above results are illustrated in the snapshots of the field profiles shown in Fig. 6. In particular we show three doublets, each depicting the profile of the gauge field (upper panel) and the scalar field (lower panel). Top, middle and bottom doublets show results for kink velocities $v_k = 0.2$, $v_k = 0.3$ and $v_k = 0.4$ respectively, for $q = 0.4$. The initial condition (gray line) at $t = t_0$ corresponds to a kink located at $x = -220$ and a bulk oscillon at $x = -150$. At t_1 a localized gauge field is shown to travel along with the domain wall, while the bulk oscillon is phase-shifted (thin black line). We also show an additional profile at t_2 (thick black line) in order to illustrate the oscillations of both nodeless and nodal solutions. From top to bottom we observe the generation of a localized gauge field with no nodes, one node and two nodes respectively.

6. Concluding remarks

In the present work we analytically obtained families of nodal and nodeless localized structures of the classical electromagnetic

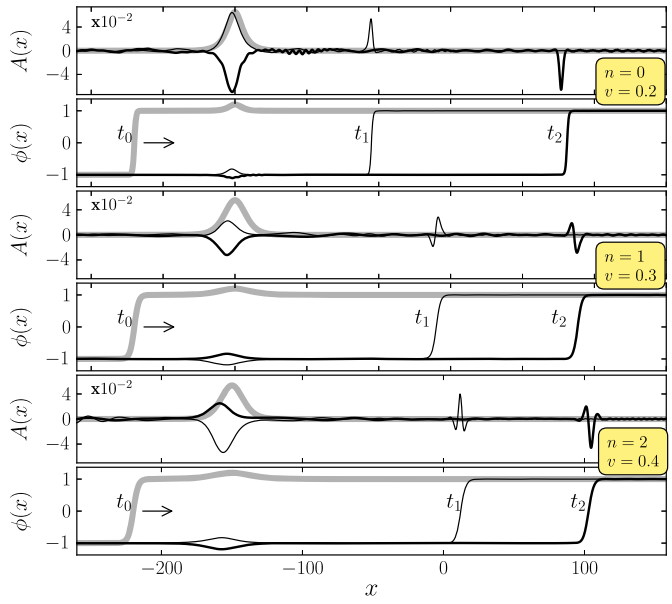

Fig. 6. (Color online.) Profiles of the fields A and ϕ for $q = 0.4$, for a collision of a moving kink with the bulk oscillons are depicted. Gray (solid) lines indicate the initial condition at $t = t_0$, before the collision takes place, while black (solid) lines at $t = t_1$ show the profiles after the dynamical localization of the gauge field at kink's core. To illustrate the oscillations that these structures undergo, profiles of both fields are also plotted at $t = t_2$. From top to bottom each field doublet refers to zero, one, and two nodes respectively while the relevant velocities of the kink are also depicted in the yellow box (bottom right of each).

sector in a $(1+1)$ dimensional setting. The interaction between the gauge and the scalar field was shown to be reduced to an effective Pöschl–Teller potential, responsible for the localization of a small amplitude gauge field.

In particular two different cases were studied: (i) a uniform vacuum $\phi = \upsilon$ and (ii) a non-uniform background (domain wall) $\phi = \upsilon \tanh\left(\sqrt{2\lambda}\upsilon x/2\right)$. In the uniform, fully higgsed-"superconducting" phase, families of small amplitude localized solutions for both fields were found, with the envelope of the scalar field satisfying a focusing NLS equation leading to sech-shaped oscillons. Accordingly, the envelope of the gauge field on a sufficiently large length scale, was found to satisfy a linear Schrödinger equation with an effective potential of the Pöschl–Teller form. Bound states of the latter, correspond to a localized gauge field with either the usual sech-shaped (nodeless) form, or the form of excited *nodal* localized structures. In a non-uniform background we also found localized gauge field solutions, stemming from an effective Pöschl–Teller potential around the kink's core. In this case however since the kink is responsible for the localization, the length-scale of the respective bound states is the same as the domain wall, which is at least an order of magnitude smaller than in the uniform case.

Numerical simulations were presented showing the long time evolution of the above obtained families of solutions, where both the ground state and excited states of the effective Pöschl–Teller potential, were found to be robust. Furthermore, by inducing a collision between the core of the domain wall and an oscillon structure in the bulk, we established a direct connection between the two different states. In this respect, the main outcome of our analysis was twofold: (i) It was demonstrated how localized fluctuations of the kink become stable. This is an important result supporting the previously described picture, concerning the dynamics close to the critical point of the spontaneous reflection symmetry breaking: the kink configuration acts as mediator of the globally broken phase since fluctuations leading to a non-vanishing value of the order parameter become stable using the kink as a background field. (ii) A dynamical mechanism for the localization of the gauge field was also demonstrated. This process may have phenomenological impact on the dynamics related to the Meissner effect close to the critical point. Thus the use of topological defects as background fields may serve as a way of driving the dynamics from the critical point and beyond and vice versa.

Appendix A. Multiscale expansion

In this section we present the MSPT expansion in more detail. We expand space–time coordinates and their derivatives as follows: $x_0 = x$, $x_1 = \epsilon x$, $x_2 = \epsilon^2 x, \ldots$, $t_0 = t$, $t_1 = \epsilon t$, $t_2 = \epsilon^2 t, \ldots$, $\partial_x = \partial_{x_0} + \epsilon\partial_{x_1} + \ldots$, $\partial_t = \partial_{t_0} + \epsilon\partial_{t_1} + \ldots$, while the asymptotic expansion for both fields is given by Eq. (12). Substituting the above expansions for the coordinates and Eq. (12) for the fields into Eqs. (8)–(9) we obtain the following equations for both ϕ and A up to order $\mathcal{O}(\epsilon^4)$:

$$\mathcal{O}(\epsilon): \hat{L}_\phi \phi^{(1)} = 0, \tag{A.1}$$

$$\mathcal{O}(\epsilon^2): \hat{L}_\phi \phi^{(2)} = -2\partial_{\mu_0}\partial^{\mu_1}\phi^{(1)} - \frac{3q^2}{2}\phi^{(1)2}, \tag{A.2}$$

$$\hat{L}_A A^{(2)} = 0, \tag{A.3}$$

$$\mathcal{O}(\epsilon^3): \hat{L}_\phi \phi^{(3)} = -2\partial_{\mu_0}\partial^{\mu_1}\phi^{(2)} - \left(\Box_1 + 2\partial_{\mu_0}\partial^{\mu_2}\right)\phi^{(1)} - 3q^2\phi^{(1)}\phi^{(2)} - \frac{q^2}{2}\phi^{(1)3}, \tag{A.4}$$

$$\hat{L}_A A^{(3)} = -2\partial_{\mu_0}\partial^{\mu_1}A^{(2)} - 2\phi^{(1)}A^{(2)}, \tag{A.5}$$

$$\mathcal{O}(\epsilon^4): \hat{L}_A A^{(4)} = -2\partial_{\mu_0}\partial^{\mu_1}A^{(3)} - \left(\Box_1 + 2\partial_{\mu_0}\partial^{\mu_2}\right)A^{(2)} - 2\left(\phi^{(1)}A^{(3)} + \phi^{(2)}A^{(2)}\right) - \phi^{(1)2}A^{(2)}, \tag{A.6}$$

where we introduced the operators $\hat{L}_\phi \equiv (\Box_0 + q^2)$ and $\hat{L}_A \equiv (\Box_0 + 1)$. The lowest order equations for the fields $\phi^{(1)}$ and $A^{(2)}$, i.e. equations (A.1) and (A.3), admit plane wave solutions given by Eqs. (13)–(14), while each satisfies the relevant dispersion relation: $\omega_1 = \sqrt{k_1^2 + q^2}$, $\omega_2 = \sqrt{k_2^2 + 1}$ respectively. In order to solve Eq. (A.2) we first eliminate the term $\sim \partial_{\mu_0}\partial^{\mu_1}$. Such a *secular* term, resonates with the operator $\hat{L}_\phi$ leading to solutions that grow linearly with time having the form: $\sim te^{iCt}$, with C the frequency of the driver. Thus, we constrain the function $u(x_i, t_i)$ by demanding that it depends on the variables x_1, t_1 only through $X_1 = x_1 - \upsilon_g^{(1)}t_1$, where $\upsilon_g^{(1)}$ is the group velocity. Taking into account this solvability condition, the form of the solution $\phi^{(2)}$ becomes:

$$\phi^{(2)} = \frac{u^2}{2}e^{-2i\omega_1 t} + \frac{u^{*2}}{2}e^{2i\omega_1 t} - 3|u|^2. \tag{A.7}$$

Continuing our analysis, to order $\mathcal{O}(\epsilon^3)$ the solvability condition leads to the following equation for the scalar field:

$$\left(\Box_1 + 2\partial_{\mu_0}\partial^{\mu_2}\right)\phi^{(1)} - 3q^2\phi^{(1)}\phi^{(2)} - \frac{q^2}{2}\phi^{(1)3} = 0. \tag{A.8}$$

Substituting in the above $\phi^{(1)}$, $\phi^{(2)}$ from equations (13) and (A.7) respectively, we obtain the NLS Eq. (15) for the envelope $u(x_1, t_2)$.

In the same order, by repeating the aforementioned arguments, and going to a frame of reference moving with group velocity $\upsilon_g^{(2)}$, the field $A^{(3)}$ becomes:

$$A_3 = \frac{2}{\Omega_+^2 - 1}uve^{-i\Omega_+ t} + \frac{2}{\Omega_-^2 - 1}uv^*e^{-i\Omega_- t} + \text{c.c}, \tag{A.9}$$

with frequency $\Omega_\pm = \omega_2 \pm \omega_1$.

Finally to order $\mathcal{O}(\epsilon^4)$ the solvability condition leads to the Schrödinger Eq. (16) for the unknown function $v(x_1, t_2)$.

References

[1] S. Coleman, Aspects of Symmetry, Cambridge University Press, 1985;
T.D. Lee, Y. Pang, Phys. Rep. 221 (1992) 251.
[2] S. Coleman, Nucl. Phys. B 262 (1985) 263;
M. Axenides, S. Komineas, L. Perivolaropoulos, M. Floratos, Phys. Rev. D 61 (2000) 085006;
R.A. Battye, P.M. Sutcliffe, Nucl. Phys. B 590 (2000) 329;
M.I. Tsumagari, E.J. Copeland, P.M. Saffin, Phys. Rev. D 78 (2008) 065021;
P. Bowcock, D. Foster, P. Sutcliffe, J. Phys. A 42 (2009) 085403.
[3] E.J. Copeland, M. Gleiser, H.-R. Muller, Phys. Rev. D 52 (1995) 1920.
[4] R. Rajaraman, Solitons and Instantons, North-Holland, Amsterdam, 1982.
[5] P.A.M. Dirac, Quantised singularities in the electromagnetic field, Proc. R. Soc. Lond. A 133 (1931) 60;
P.A.M. Dirac, Phys. Rev. 74 (1948) 817.
[6] G. 't Hooft, Nucl. Phys. B 79 (1974) 276;
A.M. Polyakov, JETP Lett. 20 (1974) 194;
A.M. Polyakov, Pis'ma Zh. Eksp. Teor. Fiz. 20 (1974) 430.
[7] P.M. Sutcliffe, Int. J. Mod. Phys. A 12 (1997) 4663.
[8] A.A. Abrikosov, Sov. Phys. JETP 5 (1957) 1174;
A.A. Abrikosov, Zh. Eksp. Teor. Fiz. 32 (1957) 1442;
H.B. Nielsen, P. Olesen, Nucl. Phys. B 61 (1973) 45.
[9] A. Vilenkin, E.P.S. Shellard, Cosmic Strings and Other Topological Defects, Cambridge University Press, UK, 2000.
[10] N. Manton, P. Sutcliffe, Topological Solitons, Cambridge University Press, Great Britain, 2004.
[11] M. Shifman, A. Yung, Phys. Rev. D 67 (2003) 125007;
M. Shifman, A. Yung, Phys. Rev. D 70 (2004) 025013.
[12] R. Auzzi, S. Bolognesi, J. Evslin, J. High Energy Phys. JHEP02 (2005) 046.
[13] P.M. Sutcliffe, Int. J. Mod. Phys. A 12 (1997) 4663;
C.J. Houghton, N.S. Manton, P.M. Sutcliffe, Nucl. Phys. B 510 (1998) 507;
B. Kleihaus, J. Kunz, Y. Shnir, Phys. Rev. D 68 (2003) 101701(R).
[14] S. Bolognesi, P.M. Sutcliffe, J. High Energy Phys. 078 (2014) 1401.
[15] M.A. Amin, E.A. Lim, I.-S. Yang, Phys. Rev. Lett. 111 (2013) 224101.
[16] T.S. Mendonça, H.P. de Oliveira, arXiv:1502.03870 [hep-th].
[17] V.A. Gani, A.E. Kudryavtsev, M.A. Lizunova, Phys. Rev. D 89 (2014) 125009.
[18] A.A. Izquierdo, M.A.G. Leön, J.M. Guilarte, Phys. Rev. D 65 (2002) 085012.
[19] V.A. Gani, A.E. Kudryavtsev, Yad. Fiz. 64 (2001) 2130, Sov. J. Nucl. Phys. 64 (2001) 2043, arXiv:hep-th/9904209.
[20] T. Fulton, R. Dynes, P. Anderson, IEEE Proc. 61 (1973) 28;
D.W. McLaughlin, A.C. Scott, Phys. Rev. A 18 (1978) 1652.
[21] B.I. Ivlev, N.B. Kopnin, Usp. Fiz. Nauk 142 (1984) 435;
B.I. Ivlev, N.B. Kopnin, Sov. Phys. Usp. 27 (1984) 206;
I.M. Dmitrenko, Fiz. Nizk. Temp. 22 (1996) 849, J. Low Temp. Phys. 22 (1996) 648.
[22] A. Valizadeh, M.R. Kolahchi, J.P. Straley, Phys. Rev. B 82 (2010) 144520.
[23] S. Brazovskii, C. Brun, Z.-Z. Wang, P. Monceau, Phys. Rev. Lett. 108 (2012) 096801.
[24] A. Moor, A.F. Volkov, K.B. Efetov, Phys. Rev. B 90 (2014) 224512.
[25] R. Jackiw, C. Rebbi, Phys. Rev. D 13 (1976) 3398.
[26] V.A. Rubakov, M.E. Shaposhnikov, Phys. Lett. B 125 (1983) 136.
[27] R. Casana, A.R. Gomes, R. Menezes, F.C. Simas, Phys. Lett. B 8 (2014) 730.
[28] D. Bazeia, J. Menezes, R. Menezes, Phys. Rev. Lett. 91 (2003) 241601.
[29] C. Callan, R. Dashen, D. Gross, Phys. Lett. B 63 (1976) 334;
S. Raby, A. Ukawa, Phys. Rev. D 18 (1978) 1154;
P. Forgács, Z. Horváth, Phys. Lett. B 138 (1983) 5.
[30] G.R. Farrar, J.W. McIntosh Jr., Phys. Rev. D 51 (1995) 5889.
[31] H. Segur, M.D. Kruskal, Phys. Rev. Lett. 58 (1987) 747.
[32] S. Flügge, Practical Quantum Mechanics, Springer-Verlag, Germany, 1999.
[33] Y. Alhassid, F. Gürsey, F. Iachello, Phys. Rev. Lett. 50 (1983) 873.
[34] P.M. Chaikin, T.C. Lubensky, Principles of Condensed Matter Physics, Cambridge University Press, UK, 2000.
[35] A. Jeffrey, T. Kawahara, Asymptotic Methods in Nonlinear Wave Theory, Pitman, London, 1982.
[36] Yu.S. Kivshar, G.P. Agrawal, Optical Solitons: From Fibers to Photonic Crystals, Academic Press, San Diego, 2003.
[37] P.G. Drazin, R.S. Johnson, Solitons: An Introduction, Cambridge University Press, Great Britain, 1989.
[38] M. Gleiser, Int. J. Mod. Phys. D 16 (2007) 219;
A. Rajantie, E.J. Copeland, Phys. Rev. Lett. 85 (2000) 916.
[39] V. Achilleos, F.K. Diakonos, D.J. Frantzeskakis, G.C. Katsimiga, X.N. Maintas, E. Manousakis, C.E. Tsagkarakis, A. Tsapalis, Phys. Rev. D 88 (2013) 045015;
F.K. Diakonos, G.C. Katsimiga, X.N. Maintas, C.E. Tsagkarakis, Phys. Rev. E 91 (2015) 023202.
[40] J. Goldstone, R. Jackiw, Phys. Rev. D 11 (1975) 1486.
[41] M. Hindmarsh, P. Salmi, Phys. Rev. D 77 (2008) 105025.
[42] N.S. Manton, Nucl. Phys. B 150 (1979) 397;
J.P. Gordon, Opt. Lett. 8 (1983) 596;
P.G. Kevrekidis, A. Khare, A. Saxena, Phys. Rev. E 70 (2004) 057603.